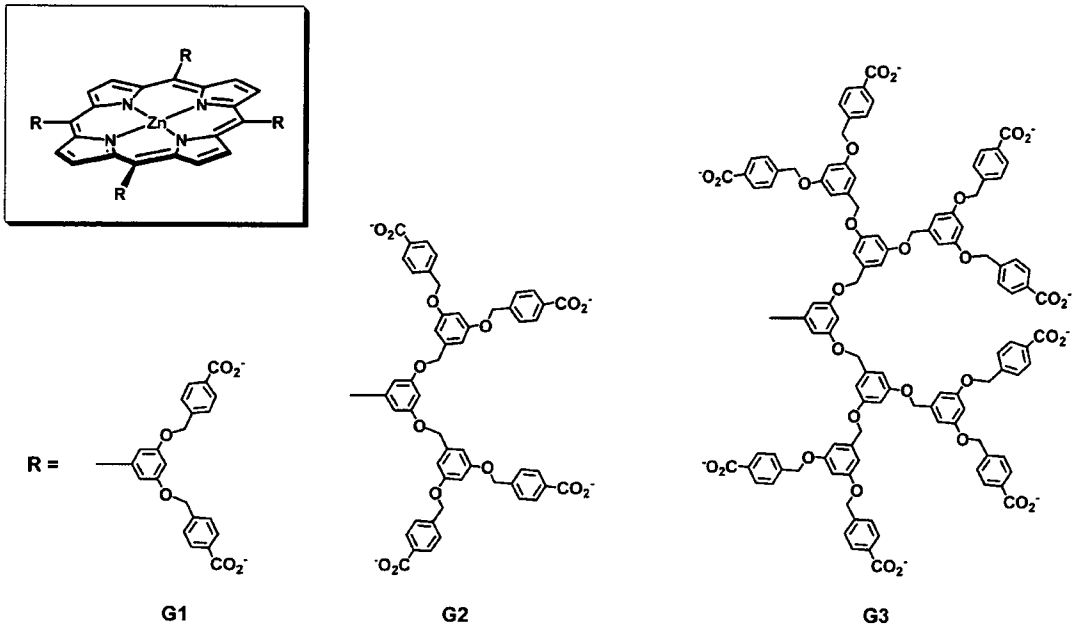

Figure 1. Structures of dendrimer porphyrins (DPs).

Table 1. Physical Properties of DP-Loaded PIC Nanocarriers

generation	hydrodynamic diameter (nm)[a]	polydispersity index (μ_2/Γ^2)	$M_{w,app}$ (10^5 g/mol)	association no. PEG-*b*-PLL/DP	CAC[b] (mg/mL)	ζ-potential (mV)
G1	126.5	0.131	2240	8989/32585	<0.1	1.11 ± 0.072
G2	78.0	0.249	100	399/722	<0.1	0.48 ± 0.31
G3	44.0	0.030	9.26	39/38	<0.1	−0.20 ± 0.57

[a] Cumulant diameter. [b] Critical association concentration.

activation by light at a wavelength matching the absorption wavelength of photosensitizer leads to the generation of reactive oxygen species (ROS) that causes the oxidative destruction of a target tissue.[12,13] As a revolutionary method in preclinical and clinical applications over the last few decades, numerous attempts have been made to improve the PDT efficacy. Among them, the creation of an efficient photosensitizer and its efficient delivery to the target tissue is an attractive topic. An ideal photosensitizer should have the following properties: (1) high quantum yield, (2) a large absorption cross-section, (3) good solubility in an aqueous medium, (4) no dark toxicity, and (5) preferential selectivity to the malignant tissue.[12−15] However, most of the photosensitizers developed in a preclinical or clinical study show poor water solubility with aggregate formation and skin phototoxicity due to a nonspecificity to tumors.[13,16]

On the basis of the above information, we have designed DPs as potential photosensitizers, because we expected that large dendritic wedges can effectively segregate the focal porphyrin cores and thereby prevent collisional quenching of the porphyrins even at a very high concentration.[9−11] In fact, the third generation DPs exhibited a remarkable PDT efficacy. In addition, ionic peripheral functionalities allow the formation of polyioncomplex (PIC) micelles with oppositely charged block copolymers.

In a present study, we investigated the systematic evaluation of the influence of the DP generation on the physicochemical properties and nanocarrier formation. A series of negatively charged DPs (Figure 1; G*n* = *n*-generation dendrimer, $n = 1-3$)[11,17,18] with poly(ethylene glycol)-*block*-poly(L-lysine) (PEG-*b*-PLL)[19−21] were used to form the PIC nanocarriers.

Results

Formation of DP-Loaded PIC Nanocarriers. The DPs were synthesized by a previously reported method.[17] All of the dendrimers were unambiguously characterized by ^{1}H NMR and MALDI-TOF-MS measurements. The DPs clearly

(9) Nishiyama, N.; Stapert, H. R.; Zhang, G.-D.; Takasu, D.; Jiang, D.-L.; Nagano, T.; Aida, T.; Kataoka, K. *Bioconjugate Chem.* **2003**, *14*, 58−66.
(10) Zhang, G.-D.; Harada, A.; Nishiyama, N.; Jiang, D.-L.; Koyama, H.; Aida, T.; Kataoka, K. *J. Controlled Release* **2003**, *93*, 141−150.
(11) Jang, W.-D.; Nishiyama, N.; Zhang, G.-D.; Harada, A.; Jiang, D.-L.; Kawauchi, S.; Morimoto, Y.; Kikuchi, M.; Koyama, H.; Aida, T.; Kataoka, K. *Angew. Chem., Int. Ed.* **2005**, *44*, 419−423.
(12) Bonnettt, R. *Chemical Aspects of Photodynamic Therapy*; Gordon and Breach Science Publishers: Amsterdam, 2000.
(13) Pandey, R. K.; Zheng, G. In *The Porphyrin Handbook*; Kadishi, R. K., Smith, K. M., Guilard, R., Eds.; Academic Press: New York, 2000; Vol. 6, pp 157−230.
(14) Derycke Annelies, S. L.; Witte, P. A. M. *Adv. Drug Delivery Rev.* **2004**, *56*, 17−30.
(15) van Dongen, G. A. M. S.; Visser, G. W. M.; Vrouenraets, M. B. *Adv. Drug Delivery Rev.* **2004**, *56*, 31−52.
(16) Hamblin, M. R.; Newman, E. L. *J. Photochem. Photobiol., B* **1994**, *23*, 3−8.
(17) Sadamoto, R.; Tomioka, N.; Aida, T. *J. Am. Chem. Soc.* **1996**, *118*, 3978−3979.
(18) Aida, T.; Jiang, D.-L. In *The Porphyrin Handbook*; Kadishi, R. K., Smith, K. M., Guilard, R., Eds.; Academic Press: New York, 2000; Vol. 3, pp 369−384.
(19) Harada, A.; Kataoka, K. *Macromolecules* **1995**, *28*, 5294−5299.
(20) Harada, A.; Kataoka, K. *Science* **1999**, *283*, 65−67.
(21) Katayose, S.; Kataoka, K. *Bioconjugate Chem.* **1997**, *8*, 702−707.

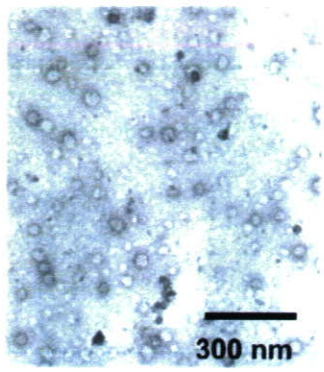

Figure 2. TEM images G3-loaded PIC nanocarriers.

formed multimolecular PIC assemblies (PIC nanocarriers) by mixing with PEG-*b*-PLL in aqueous solutions. As shown in Table 1, the DP-loaded PIC nanocarriers have almost neutral ζ-potential values, indicating a charge neutralization between the DPs and PEG-*b*-PLL to form PICs with a PEG palisade. The size and polydispersity index of the PIC nanocarriers, which were evaluated by DLS measurements, strongly depended on the generation number of the DPs (Table 1).[22] The G3-loaded PIC nanocarrier exhibits an average diameter of 44 nm and remarkably low polydispersity index ($\mu_2/\Gamma^2 = 0.030$), which is consistent with the core−shell-type micelle structure. The G2-loaded PIC nanocarrier had an average diameter of 78 nm and remarkably high polydispersity index ($\mu_2/\Gamma^2 = 0.249$), and the G1-loaded PIC nanocarrier showed a relatively large average diameter of 126 nm and a moderate polydispersity index ($\mu_2/\Gamma^2 = 0.131$). Also, the association numbers, apparent molecular weight ($M_{w,app}$), as well as the ζ-potential of the PIC nanocarriers are summarized in Table 1. The G3-loaded PIC nanocarrier was formed from 38 G3 and 39 PEG-*b*-PLL copolymers. The G2-loaded PIC nanocarrier had 1 order of magnitude higher association numbers and $M_{w,app}$ than those of the G3-loaded PIC nanocarrier. The G1-loaded PIC nanocarrier showed much higher association numbers and $M_{w,app}$ values than both the G-2 and the G-3 loaded species. The TEM image of the G3-loaded PIC nanocarriers showed spherical nanoparticles, indicating the formation of a core−shell-type micelle structure (Figure 2).

Time-Resolved Fluorescence Measurements. The aggregate formation of photosensitizers results in fluorescence quenching due to an increase in the nonradiative decay of the excited states.[23] Our previous studies[10,11] indicated that large dendritic wedges can successfully prevent the quenching of photosensitizers by steric isolation. In this context, time-resolved fluorescence decay curves of the DPs and DP-loaded PIC nanocarriers were recorded to obtain information about the effect of collisional quenching of the focal porphyrin units within the self-assembled PIC systems. As shown in Figure 3, the free DPs exhibit almost comparable fluorescent decay profiles, indicating that DPs have high solubility in aqueous medium and mostly exist in monomeric

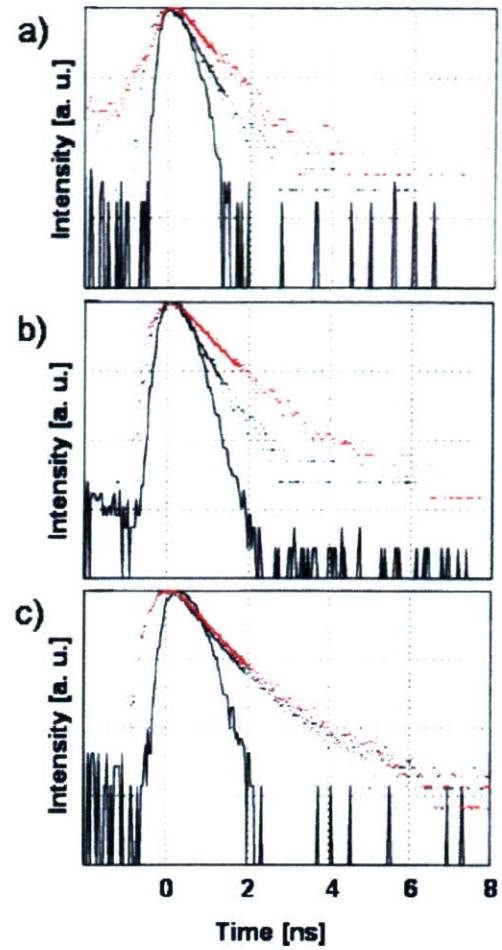

Figure 3. Fluorescence decay curves of G1 (a), G2 (b), and G3 (c) DPs (red line) and DP-loaded PIC nanocarriers (black line).

state. Within the PIC nanocarriers, the G1- and G2-loaded PIC nanocarriers exhibit a significant fluorescence quenching signature as compared to the corresponding free DPs. In sharp contrast, the G3-loaded PIC nanocarrier showed almost comparable decay rates to the free G3 (Figure 3c). This result supports our assumption that the large dendritic wedges can prevent the collisional quenching of the photosensitizing units, whereas the relatively small dendritic architecture cannot perfectly prevent the collisional quenching of the focal porphyrin units within the core of PIC nanocarriers.

Oxygen Consumption Abilities. The photoinduced oxygen consumption of the DPs and DP-loaded PIC nanocarriers was observed to evaluate the efficiency of the photochemical reactions. Under light irradiation, photosensitizers produce ROS involving singlet oxygen and the superoxide anion. The partial oxygen pressure (PO_2) change in the medium containing DPs or PIC nanocarriers with 10% FBS was recorded during photoirradiation. As shown in Figure 4, the G3 and G3-loaded PIC nanocarrier exhibit similar oxygen consumption amounts. In contrast, the oxygen consumption amount appreciably decreased when the G2 or G1 DP was loaded into the nanocarriers. Without 10% FBS, both the DPs and the DP-loaded PIC nanocarriers showed an almost negligible change in the PO_2 upon photoirradiation (data not shown),

(22) Burchard, W. In *Light Scattering: Principles and Development*; Brown, W., Ed.; Clarendon Press: New York, 1996.
(23) Lakowicz, J. R. *Principles of Fluorescence Spectroscopy*; Kluwer Academic/Plenum Publishers: New York, 1999.

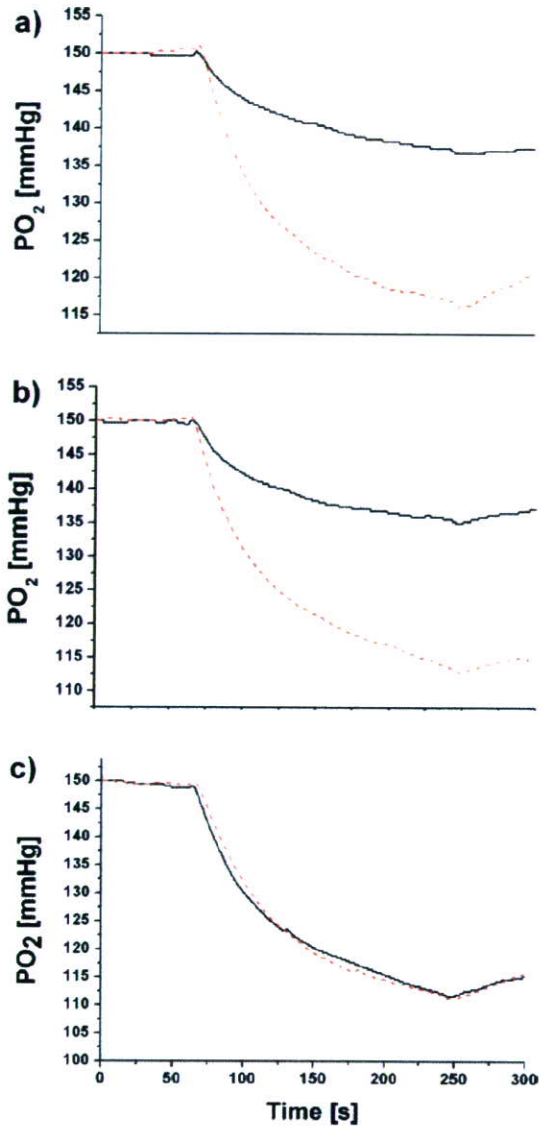

Figure 4. Oxygen partial pressure change of medium included G1 (a), G2 (b), and G3 (c) DPs (– – –) and DP-loaded PIC nanocarriers (–).

indicating that the proteins in FBS act as sacrificial acceptors of ROS.

Cellular Uptake. Efficient cellular association of a photosensitizer could lead to a high PDT efficacy. To quantitatively evaluate the cellular uptake of DPs and DP-loaded PIC nanocarriers, HeLa cells were incubated with 6.25 μM DPs or DP-loaded PIC nanocarriers having an equivalent amount of DPs (Figure 5). The cellular uptake of DPs is significantly enhanced by the incorporation into nanocarriers, indicating that the anionic surface of the DPs results in a limited interaction with a negatively charged cellular membrane. Charge neutralization and shielding of the PICs by the PEG segment might reduce the electrostatic repulsion with a cell. Therefore, encapsulation of the DPs into the PIC nanocarriers might be effective for the intracellular delivery of DPs.

The uptake amount of DPs showed a strong generation dependence. Interestingly, the G1-loaded PIC nanocarrier shows the largest uptake amount, while the G3-loaded PIC

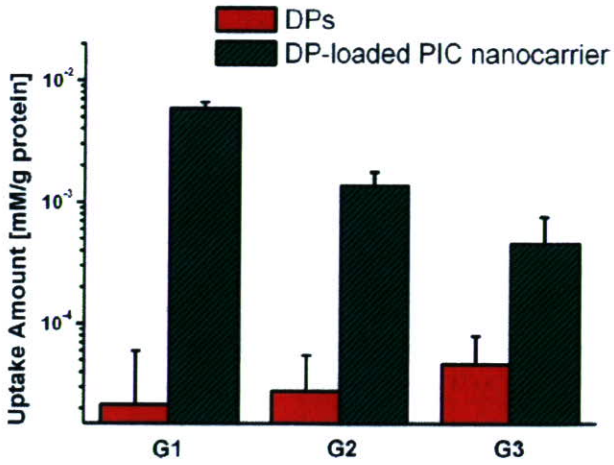

Figure 5. Cellular uptake amount of DPs and DP-loaded PIC nanocarriers. 6 μM DPs or DP-loaded PIC nanocarriers with equivalent amount of DPs is incubated.

nanocarrier gave the lowest uptake amount among the three DP-loaded PIC nanocarriers. The difference in the cellular uptake between generations is possibly caused from the morphological difference in the nanocarriers, such as the size, association number, and stability of the PICs.

Photodynamic Effect. The in vitro photodynamic effect against HeLa cells was evaluated by the MTT assay. The DPs and the DP-loaded PIC nanocarriers showed an almost negligible cytotoxicity under dark conditions (data not shown), whereas each species exhibited a strong photocytotoxicity. Figure 6 shows the cell viability–concentration curve, where the DPs apparently exhibit a remarkable increase in the photocytotoxicity by incorporation into the nanocarriers. Fifty percent inhibitory concentrations (IC_{50}) of the DPs and DP-loaded PIC nanocarriers, the concentration of photosensitizer at which 50% mortality of tumor cells as compared to the control was observed after a photoirradiation, were calculated from the cell viability–concentration curve (Table 2). The G1- and G2-loaded PIC nanocarriers exhibited 7.5 and 50 times, respectively, higher photocytotoxicities as compared to the G1 and G2 DPs. Notably, the G3-loaded PIC showed a 167 times enhanced photocytotoxicity as compared to free G3 DP.

Discussion

All of the DPs showed high solubility in aqueous medium due to the ionic charges of dendritic wedges. When the DPs are mixed with PEG-*b*-PLL copolymers in a stoichiometric ratio, positively charged PLL segments successfully interact with negative surface functionalities of DPs to form the DP-loaded PIC nanocarriers. The values of the ζ-potential also well coincide with the charge neutralization between the DPs and PEG-*b*-PLL as well as encapsulation of the PICs within the PEG layer.

Notably, the PIC nanocarriers had a high stability upon dilution with a very low critical association concentration being observed. These features are significantly important parameters from a therapeutic point of view. For target delivery of the therapeutic agent, the drug formulation should have a tolerance against dilution and maintain long circula-

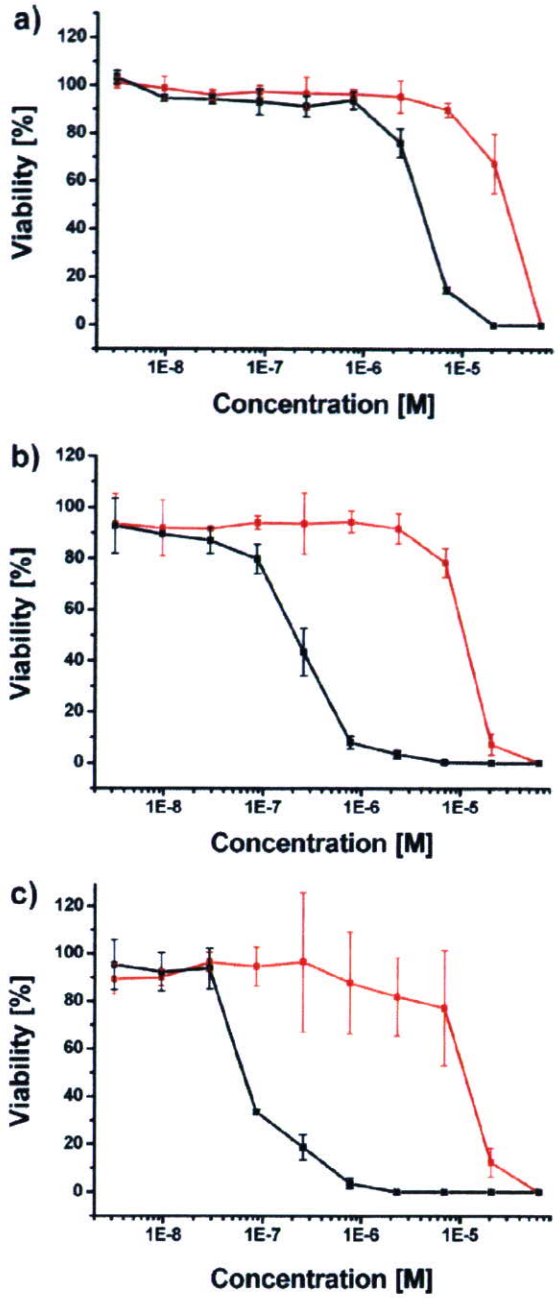

Figure 6. The viability of Hela cells treated with G1 (a), G2 (b), and G3 (c) DPs (red line) and DP-loaded PIC nanocarriers (black line).

Table 2. IC_{50} of DPs and DP-Loaded PIC Nanocarriers (unit: M)

generation	DP	DP-loaded PIC nanocarrier
G1	3.0×10^{-05}	4.0×10^{-06}
G2	1.2×10^{-05}	2.0×10^{-07}
G3	1.0×10^{-05}	6.0×10^{-08}

tion times in the blood stream. Also, the PIC nanocarriers may facilitate targeting to tumor tissues by the so-called enhanced permeability and retention (EPR) effect.[24]

The DLS measurement of the DP-loaded PIC nanocarriers exhibited a generation dependence, where the G3-loaded PIC nanocarrier showed a nicely dispersed particle formation with a diameter of 44 nm. The sizes of the G1- and G2-loaded PIC nanocarriers are generally larger than that of the G3-loaded PIC nanocarrier. TEM observations of the G3-loaded PIC nanocarrier showed a spherical assembly formation, which is consistent with the core−shell-type micelle structure. In contrast, the G2- or G1-loaded PIC nanocarrier showed a high polydispersity. The difference in size and distribution might be attributable to the number of anionic charges and dendritic architecture. The relatively open architecture of the G1 and G2 cannot perfectly prevent $\pi-\pi$ interactions among the porphyrin cores when they form the PICs. Thus, the association of the DPs with a low generation is possibly driven by the $\pi-\pi$ interaction as well as an electrostatic interaction.

In the photodynamic process sequence, the DPs are converted to excited state under light irradiation, and then they transfer excited energy or electrons to oxygen molecules to generate the ROS. The time-resolved fluorescence observation provides information about the energy transduction procedure, and the oxygen consumption ability is directly related to the ROS generation. The fluorescence decay and oxygen consumption profiles of each DP did not have large differences among the differnet generation of DPs (Figures 3 and 4). Also, the cellular uptake and photocytotoxicity of DPs were almost comparable values regardless of the generation of DPs (Figures 5 and 6). A molecular aggregation of the photosensitizers might result in the fluorescence quenching behavior. All of the free DPs exhibit almost comparable fluorescence decay profiles, indicating that DPs are succesfully segregated within aqueous medium due to high solubility and charge repulsion of surface carboxylic acid functionalities. On the other hand, the G1 and G2 showed a significant fluorescence quenching by incorporation into the PIC nanocarriers (Figure 3), indicating that the G1 and G2 have high proportions of nonradiative decays within the PIC nanocarriers by collisional quenching. Also, the G1- or G2-loaded PIC nanocarriers exhibited a significant decrease in their oxygen consumption ability as compared to the free DPs (Figure 4). We noted that either the DPs or the DP-loaded PIC nanocarrier solution without 10% FBS showed almost negligible changes in the PO_2 upon photoirradiation, indicating that the proteins in FBS act as sacrificial acceptors of the ROS. In other words, if proteins do not exist in the medium, once generated, the ROS promptly revert to the ground-state oxygen molecules due to their short lifetimes. This fact means that the reduced oxygen consumption of the G1- or G2-loaded PIC nanocarrier is possibly caused by the increase in the nonradiative decays of the excited states and also the generation of less reactive ROS. Additionally, the diffusivity of oxygen molecules is possibly reduced within the G1- and G2-loaded PIC nanocarriers due to their large hydrodynamic size. In contrast, the G3-loaded PIC nanocarrier showed an almost comparable fluorescence decay profile (Figure 3) and oxygen consumption to the free G3 (Figure 4), indicating that the third generation dendritic wedges can sufficiently prevent aggregation of the photosensitizing porphyrin units, and the G3 can efficiently transfer excited energy to oxygen molecules without loss even in a highly concentrated state of G3 in the PIC nanocarrier. Also,

(24) Maeda, H.; Wu, J.; Sawa, T.; Matsumura, Y.; Hori, K. *J. Controlled Release* **2000**, *65*, 271−284.

Table 3. The Change of Parameters of DPs by Inclusion into the PIC Nanocarriers in Each Generation System

generation	fluorescence lifetime	oxygen consumption	uptake ratio (*A*)	photocytotoxicity ratio (*B*)	*B*/*A*
G1	shortened	decreased	95	7.5	0.079
G2	shortened	decreased	53	50	0.94
G3	maintained	no change	15	167	11.1

the ROS generated from the G3-loaded PIC nanocarrier can efficiently react with serum proteins in the media.

Positively charged particles might have a large affinity against cell membranes, but the cationic particles easily associate with the negatively charged serum proteins such as albumin. Therefore, DPs with an anionic periphery may have a high availability from a clinical point of view as compared to the positively charged ones. Furthermore, the formation of the PIC nanocarriers may prevent aggregate formation during the blood circulation due to the steric stabilization of the PEG shell layer. Also, the formation of the PIC nanocarriers may improve the uptake amount of the DPs by the charge neutralization. In fact, DP-loaded PIC nanocarriers showed an appreciably high level of uptake as compared to the free DPs (Figure 5). Correspondingly, the photocytotoxicity of each PIC nanocarrier was remarkably improved as compared to that of the free DPs (Figure 6). One of the interesting aspects in this regard is the enhanced photocytotoxicity of the PIC nanocarriers encapsulating DP with an increased generation despite the generation-dependent relative decrease in their uptake amount of PIC nanocarriers.

To evaluate the effect of the DP generations on the PDT efficacy, various parameter changes after the incorporation of the DPs into the PIC nanocarriers are summarized in Table 3. The cellular uptake and photocytotoxicity ratios are obtained by normalization of the cellular uptake amount and the IC_{50} of the DP-loaded PIC nanocarriers by those of the free DPs. Additionally, the photocytotoxicity ratio is normalized by the uptake ratio for calculating the PDT efficacy of the individual DPs (*B*/*A*). G1 shows the reduced PDT efficacy by incorporation into the PIC nanocarriers. This is consistent with the shortened lifetime and decreased oxygen consumption of the G1-loaded PIC nanocarrier. However, the G2-loaded PIC nanocarrier exhibits a comparable PDT efficacy with the free G2 despite the shortened fluorescent lifetime and decreased oxygen consumption. Notably, the incorporation of the G3 into the PIC nanocarrier shows an 11-fold enhancement of the PDT efficacy. The high local concentration of DPs within the core of PIC nanocarrier is able to generate a large amount of ROS at a local site, which may lead to a high photochemical oxidation level and easily overcome the photodynamic threshold. Also, there is a possibility to change the subcellular localization of DPs by the formation of PIC nanocarriers. It should be noted in this regard that the pegylated chlorin-e6 as well as the PEG-based polymeric micelles were recently reported to show an enhanced localization in several cytoplasmic organelles including the mitochondria.[25,26] Now, we are going to observe the subcellular localization of the DPs to investigate detailed mechanism of the enhanced PDT efficacy.

Consequently, in the present investigation, we were able to determine that the PDT efficacy is highly dependent on the generation of the DPs when they formed PIC nanocarriers. The PIC nanocarriers formed from large DPs produced a high quantum yield of ROS generation and a strong nanocarrier effect, resulting in a high PDT efficacy.[27]

Conclusions

This study was conducted to systematically investigate the effect of the dendritic structures of DPs on the physicochemical property, cellular uptake, and PDT efficacy. A dendrimer generation-dependent PDT efficacy was revealed by the inclusion of DPs into supramolecular nanocarriers of PICs. To summarize the results in the present Article, we can consider the following several parameters to design effective photosensitizers: (1) Large dendritic wedges form uniform core−shell PIC micelles. (2) PIC nanocarrier formation enhances cellular uptake. (3) Incorporation of DPs in nanocarrier systems may provide enhancement of the photodynamic efficacy. In this way, G3 with a large dendritic structure encapsulated into the PIC micelles would be an ideal photosensitizer and may have a high utility for in vivo PDT applications.

Acknowledgment. This study was supported by the Industrial Technology Research Grant Program in '04 from the New Energy and Industrial Technology Development Organization (NEDO) of Japan. Y.L. acknowledges the JSPS Young Scientist Fellowship.

Supporting Information Available: Materials and detailed experimental procedures (PDF). This material is available free of charge via the Internet at http://pubs.acs.org.

CM071451M

(25) Hamblin, M. R.; Miller, J. L.; Rizvi, I.; Ortel, B.; Maytin, E. V.; Hasan, T. *Cancer Res.* **2001**, *61*, 7155−7162.
(26) Savic, R.; Luo, L.; Eisenberg, A.; Maysinger, D. *Science* **2003**, *300*, 615−618.
(27) Ideta, R.; Tasaka, F.; Jang, W.-D.; Nishiyama, N.; Zhang, G.-D.; Harada, A.; Yanagi, Y.; Tamaki, Y.; Aida, T.; Kataoka, K. *Nano Lett.* **2005**, *5*, 2426−2431.

Available online at www.sciencedirect.com
ScienceDirect
Biomaterials 28 (2007) 5169 5175
Biomaterials
www.elsevier.com/locate/biomaterials

Gene delivery with biocompatible cationic polymer: Pharmacogenomic analysis on cell bioactivity

Kayo Masago[a,1], Keiji Itaka[a,1], Nobuhiro Nishiyama[a], Ung-il Chung[a,c,d], Kazunori Kataoka[a,b,d,*]

[a]*Division of Clinical Biotechnology, Center for Disease Biology and Integrative Medicine, Graduate School of Medicine, The University of Tokyo, Japan*
[b]*Department of Materials Science and Engineering, Graduate School of Engineering, The University of Tokyo, Japan*
[c]*Department of Bioengineering, Graduate School of Engineering, The University of Tokyo, Japan*
[d]*Center for Nanobio Integration, The University of Tokyo, 7-3-1 Hongo, Bunkyo-ku, Tokyo 113-0033, Japan*

Received 7 June 2007; accepted 10 July 2007
Available online 30 July 2007

Abstract

The availability of non-viral gene delivery systems is determined by their capacity and safety during gene introduction. In this study, the safety issues of polyplex were analyzed from the standpoint of the biomolecular mechanisms. P[Asp(DET)], a newly developed polymer, polyasparagine carrying the *N*-(2-aminoethyl)aminoethyl group as the side chain which was recently revealed to show good transfection efficiency to primary cells, was compared to conventional linear poly(ethylenimine) (LPEI). After transfection toward a bioluminescent cell line, P[Asp(DET)] maintained the expression level of stably expressing luciferase. In contrast, LPEI showed a decrease in the luciferase expression, while the similar expression of exogenous reporter gene was obtained. Evaluation of the housekeeping genes expression as well as the profiles of pDNA uptake after transfection suggested the time-dependent toxicity of LPEI that perturbs cellular homeostasis. Consistently, the induction of osteogenic differentiation by functional gene introduction was achieved only by P[Asp(DET)], even though appreciable expression of the gene was achieved by LPEI. It is crucial that this aspect of safety be taken into account, especially when the gene introduction is applied to primary cells to regulate such cell function as differentiation. This biomolecular analysis focusing on cellular homeostasis is beneficial for assessing the practicability of the gene delivery systems for clinical application.

Keywords: Biocompatibility; Gene transfer; Cationic polymer; Cytotoxicity; Cell differentiation

1. Introduction

Gene therapies have attracted progressive attention for the treatment of numerous intractable diseases, but the lack of safe and efficient gene-delivery systems is an obstacle to their clinical application. Viral vectors are known to be highly potent gene delivery systems, yet may also induce adverse side effects, including severe immunological and toxicological responses. In fact, recent clinical trials using viral vectors have been halted due to unprecedented toxicity, including the death of a patient [1–4]. Therefore, non-viral gene carriers such as cationic lipids and polymers are expected to be an alternative to viral vectors directing therapeutic genes to target tissues.

The availability of gene carriers is largely determined by their transfection efficiency and cytotoxicity. Although the latter is generally evaluated through the viability assay of cultured cells such as an MTT assay [5], an MTT assay only reflects the non-specific outcome of cell death. Synthetic carriers may induce side effects including complement activation, carcinogenicity, teratogenicity and immunogenicity, all of which are serious concerns for clinical application [6]. Thus, the safety issues of non-viral gene carriers, both on a cellular and systemic basis,

*Corresponding author. Department of Materials Engineering, Graduate School of Engineering, The University of Tokyo, 7-3-1 Hongo, Bunkyo-ku, Tokyo 113-0033, Japan. Tel.: +81 3 5841 7138; fax: +81 3 5841 7139.
E-mail address: kataoka@bmw.t.u-tokyo.ac.jp (K. Kataoka).
[1]These authors contributed equally to this work.

0142-9612/$ - see front matter © 2007 Elsevier Ltd. All rights reserved.
doi:10.1016/j.biomaterials.2007.07.019

are critical for their clinical development, requiring careful analysis of the toxicity by exploring the biomolecular mechanisms. In this regard, a pharmacogenomic analysis of the global gene expression in the transfected cells is of particular interest. This approach has recently been advocated as polymer genomics or material genomics, and several studies have been reported to have applied it for the evaluation of non-viral gene carriers [7,8].

Recently, we developed a novel block catiomer-based gene delivery system that showed excellent capacity for *in vitro* transfection to primary cells [9]. This system is composed of plasmid DNA (pDNA) and poly(ethyleneglycol)-block-polyasparagine carrying the *N*-(2-aminoethyl) aminoethyl group $(CH_2)_2NH(CH_2)_2NH_2$ as the side chain (PEG-PAsp[DET]). Ethylene diamine units located at the side chain are only half protonated under neutral pH and are thus feasible candidates to perform the so-called proton sponge effect, which has been believed to be the major mechanism for the excellent transfection efficiency of some polyamine derivatives having substantially lowered pKa such as poly(ethylenimine) (PEI) [10–12]. As well as the good transfection efficiency, the polyplex micelles from this block catiomer showed minimal cytotoxicity toward various primary cells, achieving the successful *in vivo* gene introduction to the vascular lesions [13] and the effective induction of cell differentiation both *in vitro* and *in vivo* through the effective expression of the genes encoding transcriptional factors [14].

These results motivated us to perform an additional toxicogenomic study of P[Asp(DET)] in order to ensure the safety for future clinical application. Linear PEI (LPEI) was used as a control, representing the common polycation for the construction of polyplexes. Although P[Asp(DET)] and LPEI both have a buffering capacity under an endosomal pH, they showed a considerable difference in the toxicological profiles which revealed the appreciably lowered toxicity of the former compared to the latter. In particular, the time-dependent change in the pharmacogenomical toxicity toward the targeted cells was evaluated in detail, in regards to the capacity of inducing cell differentiation through the transfection of functional genes encoded in the encapsulated pDNA in the polyplex.

2. Materials and methods

2.1. Materials

pGL3-control pDNA encoding firefly luciferase (Promega, Madison, WI, USA), pRL-CMV pDNA encoding renilla luciferase (RL) (Promega), and EGFP-C1 pDNA encoding EGFP (Clontech, Palo Alto, CA, USA) were amplified in the *Escherichia coli* strain DH5α, which was isolated and purified using a QIAGEN HiSpeed Plasmid Maxi Kit (Qiagen, Hilden, Germany). pCMV5 pDNA expressing HA-tagged mouse caALK6 and pcDEF3 pDNA expressing Flag-tagged mouse Runx2 were generous gifts from Dr. M. Krüppel (Mt. Sinai Hospital, Toronto, ON, Canada) and Dr. K. Miyazono (University of Tokyo, Tokyo, Japan), respectively. The concentration of DNA was determined by measuring the UV absorption at 260 nm.

2.2. Cells

HuH-7 cells were obtained from the Riken Cell Bank (Tsukuba, Japan). Bioluminescent cells (HuH-7-luc) stably expressing firefly luciferase were kindly provided by Mr. S. Matsumoto (University of Tokyo). Dulbecco's modified Eagle's medium (DMEM) and fetal bovine serum (FBS) were purchased from Sigma-Aldrich (St. Louis, MO, USA).

2.3. Polycations for the preparation of polyplex

LPEI (Exgen 500, $M_w = 22$ kDa) was purchased from MBI Fermentas (Burlington, ON, Canada). Diethylenetriamine (DET) was purchased from Tokyo Kasei Kogyo (Tokyo, Japan). All other chemicals were purchased from Wako Pure Chemical Industries (Osaka, Japan). P[Asp(DET)] was synthesized by the side-chain aminolysis reaction of the poly (β-benzyl L-aspartate) (PBLA) as previously reported [9]. Briefly, the PBLA was synthesized by the ring-opening polymerization of the β-benzyl-L-aspartate *N*-carboxyanhydride (BLA-NCA) initiated by the primary amine of *n*-butylamine in *N,N*-dimethylformamide (DMF)/dichloromethane (1:10) at 40 °C, followed by the acetylation of the *N*-terminal amine with acetic anhydride. Gel permeation chromatography (GPC) was performed to confirm a unimodal molecular weight distribution (M_w/M_n 1.20) of PBLA by TOSHO HLC-8220 (columns: TSK-gel G4000HHR + G3000HHR, eluent: DMF + 10 mM LiCl, $T = 40$ °C, detector: refractive index). The degree of polymerization of PBLA was determined as 98 from the ^{1}H NMR spectrum (JEOL EX300 spectrometer: JEOL, Tokyo, Japan). Then, the side-chain aminolysis reaction of PBLA was performed by mixing the DMF solution of PBLA(50 mg/ml) with a 50-fold excess of DET in DMF at 40 °C to obtain P[Asp(DET)].

2.4. Polyplex formation

Each polyplex sample with a pDNA concentration of 33 μg/mL was prepared by simply mixing pDNA and polycation(LPEI or P[Asp(DET)]) at the indicated *N/P* ratio (= [total amines in polycation]/[DNA phosphates]) in a 10 mM Tris HCl (pH 7.4) buffer solution.

2.5. Dual luciferase measurement on HuH-7-luc cells transfected with pRL-CMV pDNA

HuH-7-luc cells were seeded on 96-well culture plates (3×10^3 cells/well) and incubated overnight in 100 μl DMEM supplemented with 10% FBS and penicillin/streptomycin. After the culture medium was replaced with fresh medium containing 10% FBS, 5.5 μl of the polyplexes composed of P[Asp(DET)] or LPEI (final DNA concentration: 33 μg/ml) were applied to each well. After 24 h, the medium was changed to remove the polyplexes, followed by further incubation for 24 or 48 h. The firefly and RL activities were measured using a Dual-Luciferase Reporter Assay System (Promega) according to the protocol provided by the manufacturer, using a GloMax™ 96 Microplate Luminometer (Promega).

2.6. Cell proliferation assay

HuH-7-luc cells (6×10^4 cells/well) were seeded in six-well plates and cultured overnight. After the transfection as described above (polyplex solution: 90 μl/well), the cells were washed with phosphate-buffered saline (PBS), trypsinized, and scraped off. Then the cell number was counted by a nucleo counter (Chemometec, Tokyo, JAPAN) following the protocol provided by the manufacturer. The measurement was duplicated.

2.7. Lactate dehydrogenase (LDH) assay

The degree of membrane destabilization was examined by lactate dehydrogenase (LDH) activity liberated from the cytoplasm. The cells were plated on 96-well plates and incubated overnight in 100 μl of DMEM

containing 10% FBS. Then the medium was changed and 5.5 μl of polyplex was added to each well similarly as in the transfection described above. After 4, 8, or 24 h, the plates were centrifuged for 5 min at 110*g*. Then, 50 μl of aliquots in each well were collected and subjected to the LDH measurement. A CytoTox 96 Non-Radioactive Cytotoxicity Assay kit (Promega) was used following the protocol provided by the manufacturer, using a plate reader AD200 (Beckman Coulter, Inc., USA) for reading the OD at 490 nm to determine the amount of the produced diformazan. Freeze-chaw cells were used to calibrate 100% LDH activity. To compare the cytotoxicity between P[Asp(DET)] and LPEI, the parametrical analysis using the Student's *t*-test was performed.

2.8. Quantitative assay on the cellular uptake of pDNA by real-time quantitative PCR

EGFP-C1 pDNA expressing EGFP was transfected to HuH-7. 8×10^4 HuH-7 cells/well were plated in six-well plates and cultured overnight, and then the transfection was done similarly as described before. At the indicated time periods (4, 8 and 24 h), the DNA was collected and purified from each well using a Wizard Genomic DNA purification Kit (Promega), then subjected to the PCR for the quantification of pDNA copies encoding EGFP. The copy number of β-actin (βA) was also determined by the ABI 7500 Fast Real-Time PCR systems to normalize the cell number (Applied Biosystems, Foster City, CA, USA). The sequences of the primers and probe used for EGFP were as follows: forward primer GGGCACAAGCTGGAGTACAAC and reverse primer TCTGCTT GTCGGCCATGATA. The sequence of the probe was ACAGCCA CAACGTCT with FAM as a fluorescent dye on the 5-end and MGB as a fluorescence quencher dye labeled on the 3-end. For βA amplification and quantitation, the forward and reverse primers and probe were purchased as a standard TaqMan gene expression assay kit from Applied Biosystems. PCR was done for 20 s at 95 °C, followed by 3 s at 95 °C and 60 s at 60 °C for 40 cycles. A linear relationship between the number of cells and threshold cycle for the βA gene amplification was confirmed (data not shown).

2.9. Evaluation of osteocalcin mRNA expression

Osteogenic differentiation of the mouse calvarial cells was evaluated by the expression of osteocalcin mRNA, an osteoblast-differentiation marker. Mouse calvarial cells were isolated from the calvariae of neonatal littermates. The experimental procedures were handled in accordance with the guidelines of the Animal Committee of the University of Tokyo. Calvariae were digested for 10 min at 37 8 °C in an enzyme solution containing 0.1% collagenase and 0.2% dispase for five cycles. Cells isolated by the final four digestions were combined and cultured in DMEM supplemented with 10% FBS and penicillin/streptomycin. For induction of the differentiation assays, 3×10^4 primary mouse calvarial cells were plated in six-well culture plates and cultured for 24 h. After changing the medium to that containing 10% FBS and dexamethazone, polyplexes containing pDNAs expressing caALK6 and Runx2 were applied to each well by a similar transfection procedure as that previously described. The culture medium was refreshed on Day 3 after transfection, then changed every 3 days. On Days 5 and 11, the cells were washed with PBS and the total RNA was collected using the RNeasy Mini Preparation Kit (Qiagen) according to the manufacturer's protocol. Gene expression was analyzed by a quantitative PCR. 500 ng of total RNA was analyzed in a final volume of 50 μl. Reverse transcription was performed for 30 min at 50 °C followed by PCR: 50 °C for 2 min, 95 °C for 10 min, followed by 40 cycles of 95 °C for 15 s and 60 °C for 1 min using the Quantitect SYBR Green PCR Kit (Qiagen). Each mRNA expression was normalized to levels of mouse βA mRNA. The primers used were as follows: osteocalcin: forward primer (AAGCAGGAGGGCAATAAGGT) and reverse primer (TTTGTAGGCGGTCTTCAAGC); mouse βA: forward primer (AGATGTGGATCAGCAAGCAG), reverse primer (GCGCAAGT-TAGGTTTTGTCA). To compare the osteocalcin expressions using P[Asp(DET)] or LPEI, the parametrical analysis using the Student's *t*-test was performed.

2.10. Housekeeping gene expression assay

After a similar transfection procedure as previously described was performed, the total RNA was collected at 24 or 72 h. To evaluate the expressions of the housekeeping genes, a Taqman Human Endogenous Control Plate (Applied Biosystems) was used according to the manufacturer's protocol, including 18S rRNA, acidic ribosomal protein (PO), βA, cyclophilin (CYC), glyceraldehyde-3-phosphate dehydrogenase (GAPDH), phosphoglycero-kinase (PGK), β2-microglobulin (β2m), β-glucronidase (GUS), hypoxanthine ribosyl transferase (HPRT), TATA binding protein (TBP) and transferrin receptor (TfR). The control cells serve as a baseline for the assays and are shown as zero on the graph. The results are expressed in the comparative cycle threshold; ΔC_T, greater than or less than the control ΔC_T.

3. Results and discussion

3.1. In vitro transfection toward bioluminescent cell line

The bioluminescent human hepatoma cell line (HuH-7-Luc) stably expressing firefly luciferase (Luc) was used to evaluate the pharmacogenomic influence as well as the transfection efficiency of the polyplexes. After the transfection of RL using P[Asp(DET)] or LPEI, both the Luc and RL expressions were estimated simultaneously. The expressions were normalized by the number of cells, which were directly counted after scraping the cells from the culture plates.

The exogenous RL expressions per cell in Fig. 1(a) showed that the P[Asp(DET)] polyplex had comparable transfection efficiency to the LPEI polyplex giving the highest expression at 48 h after transfection. In contrast, the endogenous Luc expression showed a different profile between the two polyplexes; the Luc expression of the cells transfected by the P[Asp(DET)] polyplex was equivalent as that of the control cells, while the cells transfected by the LPEI polyplex showed a gradual decrease in Luc expression per cell (Fig. 1(b)). The cell numbers shown in Fig. 1(c) revealed that the proliferation was significantly inhibited by the transfection using LPEI after Day 2, compared to that of the other two groups (the cells transfected by P[Asp(DET)] and the control). Note that in these experiments, the polyplexes in the medium were removed at 24 h after transfection by changing the culture medium. Thus, these results suggest that although the exogenous RL gene expression showed an increase until Day 2, the internalized LPEI into the target cells by Day 1 had some continuous inhibiting effects on the proliferation and endogenous gene expression in the targeted cells. It is reasonable to assume that the LPEI released from the polyplex may impair the intracellular activities in a time-dependent manner.

3.2. Investigation of the cytotoxicity induced by LPEI

To investigate the detailed mechanisms of the time-dependent cytotoxicity possibly induced by LPEI, we

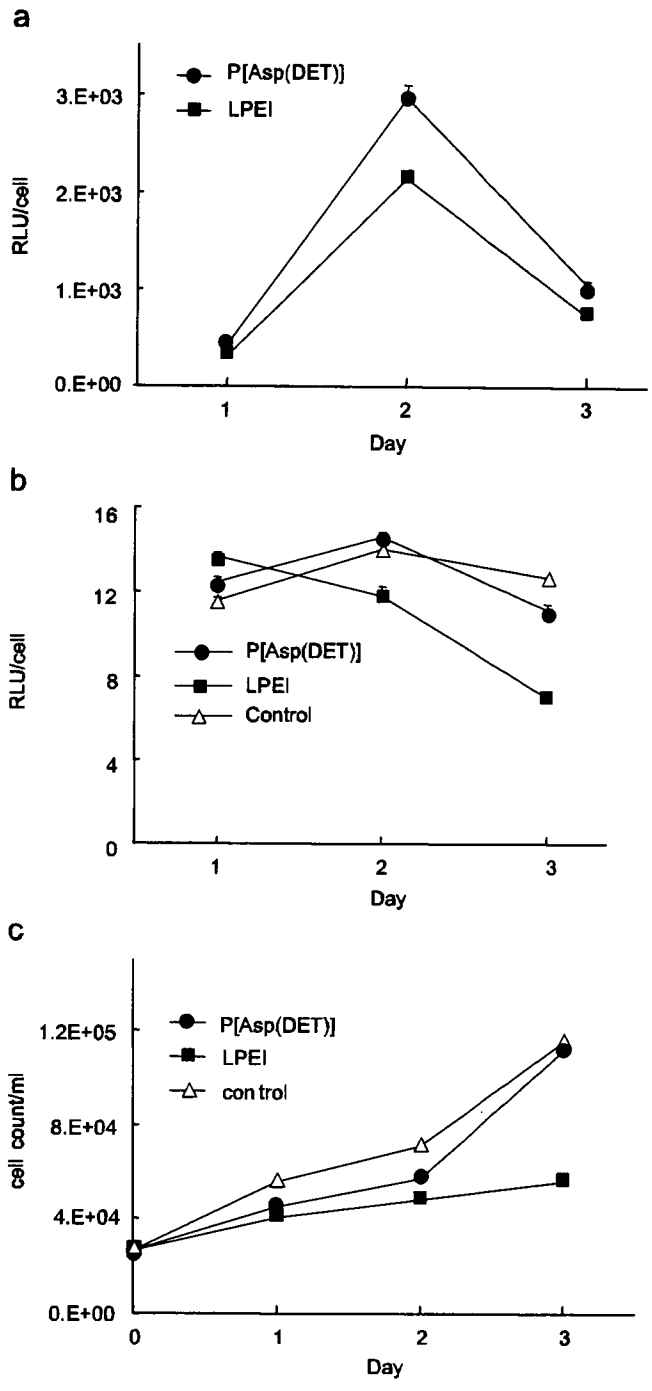

Fig. 1. *In vitro* transfection toward HuH-7-Luc cells. (a) Exogenous renilla luciferase expression. (b) Endogenous firefly luciferase expression. (c) Cell proliferation assay. Transfection was performed by P[Asp(DET)] (closed circle) or LPEI (closed square) polyplexes formed at $N/P = 10$. Gene expression was evaluated for 3 days after transfection and normalized by the cell number. Each data of gene expression represents mean ± SD ($n = 8$). The data of cell number are means ($n = 2$).

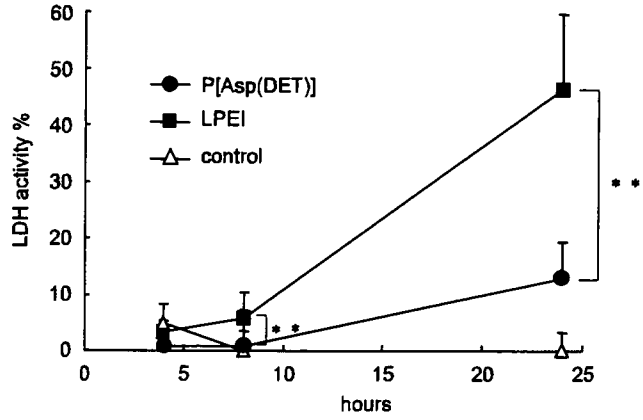

Fig. 2. Evaluation of LDH activity after transfecton using P[Asp(DET)] (closed circle) or LPEI (closed square) polyplexes. Each data represents mean ± SD ($n = 8$). Freeze-chaw cells were used to calibrate 100% LDH activity. $^{**}P<0.01$.

further assessed each step involved in the transfection process. The first step is apparently the cellular association and internalization of the gene carriers. It is assumed that these events may evoke membrane destabilization, possibly causing cytotoxic effects [15]. The change in membrane permeability due to the interaction with the polyplexes was examined by an LDH assay under the same condition as used in the transfection experiments above. As presented in Fig. 2, the cells transfected by the LPEI polyplex revealed a time-dependent increase in the leakage of LDH until 24 h after transfection. In contrast, the P[Asp(DET)] polyplex induced a minimal LDH leakage compared to the control. Considering the similar cationic nature of LPEI and P[Asp(DET)], the membrane destabilization after their association onto the plasma membrane is expected to be similar, which is apparently not the case observed here. The discrepancy between the two polymers on the time-dependent LDH leakage suggests that factors other than simple electrostatic interaction play a substantial role in the process of membrane destabilization.

The uptake amount of reporter gene into the HuH-7 cells by the P[Asp(DET)] or LPEI polyplex was determined by a real-time PCR in terms of gene copies per cell from the total DNA samples [16–18]. As seen in Fig. 3(a), the uptake amount of reporter gene showed a continuous increase until 24 h after the transfection in the case of the P[Asp(DET)] polyplex. The amount of reporter genes internalized with the LPEI polyplex was similar to that with the P[Asp(DET)] polyplex at 8 h, yet was significantly reduced by extending the transfection time to 24 h. One possible reason for this phenomenon might be the rapid dissociation of pDNA from LPEI in the cytoplasm as reported in the literature [19], resulting in its fast degradation by cytoplasmic enzymes [20,21]. However, when the culture medium was changed to remove the polyplexes at 4 h after the transfection, both systems showed a similar profile of a gradual decrease in the copy number after the medium change (Fig. 3(b)), suggesting the similar stability of the internalized pDNAs for both systems. These results suggest that the decrease in the internalized amount of the reporter gene with the LPEI polyplex shown in Fig. 3(a) may be due to

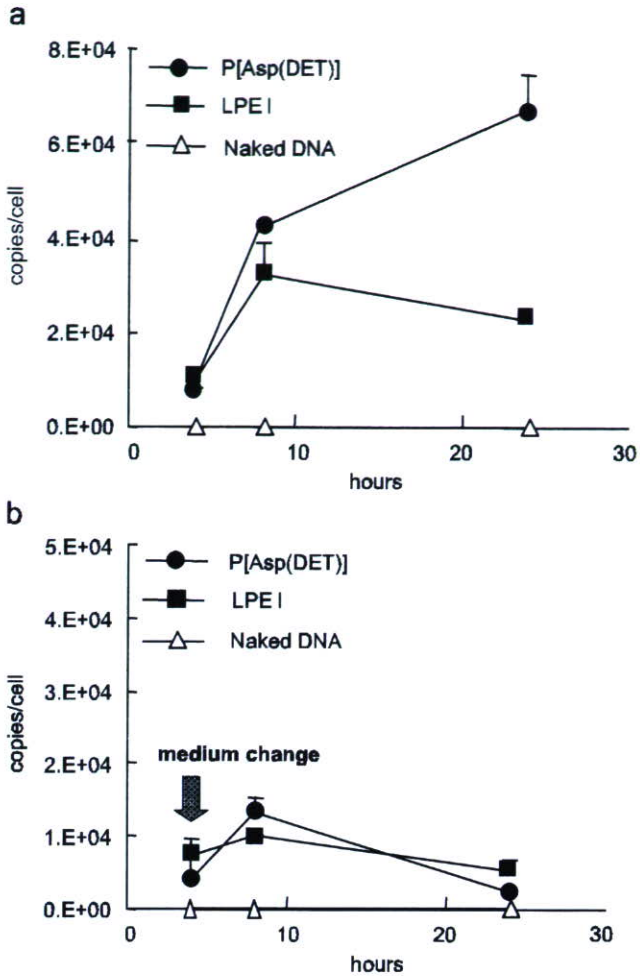

Fig. 3. Evaluation of pDNA uptake after transfecton using P[Asp(DET)] (closed circle), LPEI (closed square), or by the form of naked pDNA (open triangle). The cellular uptake of pDNA was quantified by a PCR, (a) without changing medium during the procedure, or (b) with medium change after 4 h of transfection. Each data represents mean ± SD ($n = 3$).

the time-dependent decrease in the cellular activity to take up the polyplexes caused by the toxicity of LPEI.

To clarify this possible time-dependent influence on the cellular function from the viewpoint of the genomics, we assessed the change in the gene expressions of 11 frequently used housekeeping genes in the presence of the polyplex. These genes usually revealed a uniform expression, but the expression profile may vary in response to various external factors such as stress on the cells [22,23]. Thus, the variation in their expression profile is a good indicator for assessing the cellular function, a possible perturbation in the cellular homeostasis. The quantitative evaluation of the expression of these housekeeping genes by a real-time PCR revealed that the cells transfected by LPEI apparently showed downregulation in the expression of the housekeeping genes at 72 h after the transfection (Fig. 4(b)). Although the measurement at 24 h showed minimal fluctuation in the housekeeping gene expression, GAPDH and CYC were significantly downregulated by more than

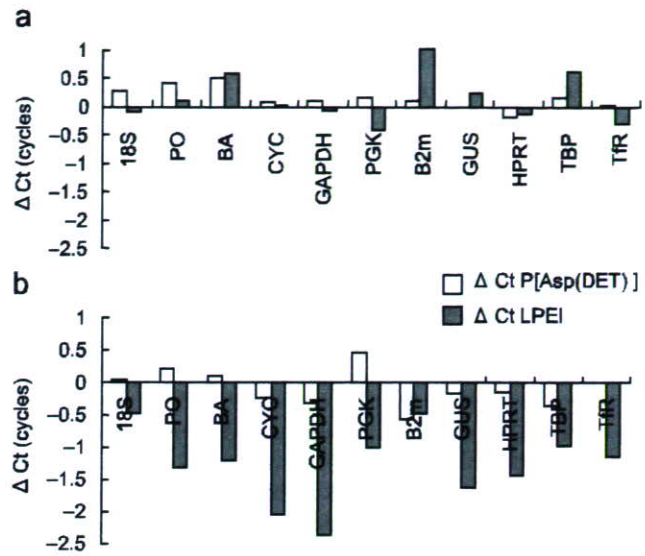

Fig. 4. Housekeeping genes expression after transfection. The mRNA expressions of various housekeeping genes were evaluated by a quantitative PCR at (a) 24 h and (b) 72 h after transfection using P[Asp(DET)] (open bar) or LPEI (filled bar).

two cycles of ΔC_T values compared to those of the control cells at 72 h, indicating a four-fold decrease in gene expression. In these assays, the culture medium was changed at 24 h. Thus, it is likely that LPEI associated with the cells may induce the perturbed gene expression through the continuous interaction with intracellular components even after the medium change at 24 h to remove excess polyplexes in the medium. In contrast, the expression of these genes in the cells transfected by P[Asp(DET)] retained constant even after 72 h, all of which were within 0.5 cycles compared to those of the control cells. These results of the housekeeping gene expressions suggest the sustained homeostasis through the transfection process using P[Asp(DET)], leading to constant cellular activity such as the polyplex uptake (Fig. 3(a)), proliferation (Fig. 1(c)), and continuous gene expression (Fig. 1(b)).

As was occasionally reported, polyplexes induce critical cytotoxicity especially at higher N/P ratios, presumably due to the presence of free polymers [24–26]. Although the mechanisms are likely to involve various cellular responses such as immunostimulation [27] and apoptosis [15,28], the plasma membrane perturbation associated with the cationic polymers may be an initial event that induces the toxicity [28,29]. From our present results on LDH release (Fig. 2), the disorder on the plasma membrane seems to occur within 24 h after the transfection with the LPEI polyplex. In addition, the intracellular events that were noticed as the change in the endogenous gene expressions emerged after 72 h of transfection. It should be noted that these events of the perturbed expression of endogenous genes were inevitable even after further supply of the polyplexes was halted by the medium change at 24 h, strongly suggesting that the free PEI remaining inside the

cells after the polyplex dissociation may cause an unfavorable interaction with the intracellular components in a time-dependent manner.

3.3. Transfection toward mouse calvarial cells and induction of osteogenic differentiation

The data so far indicates the minimal cytotoxicity of P[Asp(DET)], suggesting a feasible capacity in gene delivery for therapeutic purposes. To assess this feasibility, we evaluated the induction of cell differentiation by exogenous gene introduction. pDNAs encoding bioactive factors, caALK6 and Runx2, both of which were revealed to induce the effective osteogenic differentiation [30], were introduced in this way to mouse calvarial cells derived from neonatal calvariae. The osteogenic differentiation was evaluated by the expression of osteocalcin mRNA, a specific osteoblast-differentiation marker. As shown in Fig. 5, the time-dependent increase in osteocalcin expression was confirmed after the transfection of caALK6+Runx2 using P[Asp(DET)]. In contrast, no sign of the osteocalcin expression was observed by the LPEI polyplex until Day 11. Notably, the GFP-encoding pDNA, a negative control of differentiation, achieved almost identical GFP expression by the P[Asp(DET)] and LPEI polyplexes, without apparent morphologic changes in the targeted cells as observed under the microscope (data not shown). It can be reasonably assumed that, with the same transfection procedure, the osteogenic factors of caALK6 and Runx2 were also expressed similarly inside the targeted cells by the P[Asp(DET)] and LPEI polyplexes. Therefore, the lack of osteocalcin induction by the LPEI polyplex is considered to be due to the adverse effect on cell bioactivity by LPEI. In contrast, P[Asp(DET)] was revealed to be available for practical use in the induction of cell differentiation.

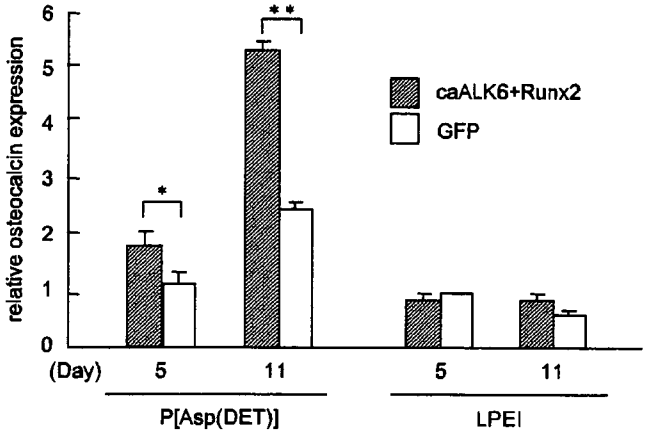

Fig. 5. Evaluation of osteocalcin mRNA expression by a quantitative PCR. Osteogenic differentiation was induced on the mouse calvarial cells by transfection of caALK6 and Runx2 (hatched bar) using P[Asp(DET)] or LPEI. As a negative control, a GFP (open bar) gene was used. After 5 or 11 days of transfection, the total RNA was collected and the osteocalcin expression was estimated. Each data represents mean±SD ($n = 3$). $^{*}P<0.05$ and $^{**}P<0.01$.

4. Conclusions

In conclusion, although LPEI has been widely used for gene introduction to various cell lines, the time-dependent cytotoxicity, which perturbs cellular homeostasis, should be carefully considered even though an appreciable expression of the reporter gene was achieved. As exemplified here in the osteogenic differentiation, impaired cellular function gave a negative effect in the intracellular signal transduction directing cell differentiation. This aspect of toxicity should be carefully counted especially when gene therapy is proposed to promote such cell functions as differentiation. Worth noting in this regard is the excellent capacity of the gene introduction of P[Asp(DET)] with minimal toxic effects, indicating that this system holds much promise for the therapeutic applications of gene therapy requiring safe and regulated gene expressions.

Acknowledgments

We thank Dr. M. Krüppel and Dr. K. Miyazono for pDNAs expressing caALK6 and Runx2, respectively. This work was supported by Grants-in-Aid for Scientific Research from the Japanese Ministry of Education, Culture, Sports, Science and Technology (#15390452 and #17390412), Health Science Research Grants from the Japanese Ministry of Health, Labor and Welfare (#H17-Immunology-009), and the Core Research Program for Evolutional Science and Technology (CREST) from the Japan Science and Technology (JST) Agency.

References

[1] Marshall E. Gene therapy death prompts review of adenovirus vector. Science 1999;286(5448):2244 5.
[2] Hollon T. Researchers and regulators reflect on first gene therapy death. Nat Med 2000;6(1):6.
[3] Assessment of adenoviral vector safety and toxicity: report of the National Institutes of Health Recombinant DNA advisory committee. Hum Gene Ther 2002;13(1):3 13.
[4] Gansbacher B. Report of a second serious adverse event in a clinical trial of gene therapy for X-linked severe combined immune deficiency (X-SCID). Position of the European Society of Gene Therapy (ESGT). J Gene Med 2003;5(3):261 2.
[5] Mosmann T. Rapid colorimetric assay for cellular growth and survival: application to proliferation and cytotoxicity assays. J Immunol Methods 1983;65(1 2):55 63.
[6] Duncan R. The dawning era of polymer therapeutics. Nat Rev Drug Discov 2003;2(5):347 60.
[7] Omidi Y, Hollins AJ, Benboubetra M, Drayton R, Benter IF, Akhtar S. Toxicogenomics of non-viral vectors for gene therapy: a microarray study of lipofectin- and oligofectamine-induced gene expression changes in human epithelial cells. J Drug Target 2003;11(6): 311 23.
[8] Kabanov AV, Batrakova EV, Sriadibhatla S, Yang Z, Kelly DL, Alakov VY. Polymer genomics: shifting the gene and drug delivery paradigms. J Control Release 2005;101(1-3):259 71.

[9] Kanayama N, Fukushima S, Nishiyama N, Itaka K, Jang WD, Miyata K, et al. A PEG-based biocompatible block catiomer with high buffering capacity for the construction of polyplex micelles showing efficient gene transfer toward primary cells. Chem Med Chem 2006;1(4):439 44.

[10] Boussif O, Lezoualc'h F, Zanta MA, Mergny MD, Scherman D, Demeneix B, et al. A versatile vector for gene and oligonucleotide transfer into cells in culture and in vivo: polyethylenimine. Proc Natl Acad Sci USA 1995;92(16):7297 301.

[11] Boletta A, Benigni A, Lutz J, Remuzzi G, Soria MR, Monaco L. Nonviral gene delivery to the rat kidney with polyethylenimine. Hum Gene Ther 1997;8(10):1243 51.

[12] Goula D, Benoist C, Mantero S, Merlo G, Levi G, Demeneix BA. Polyethylenimine-based intravenous delivery of transgenes to mouse lung. Gene Ther 1998;5(9):1291 5.

[13] Akagi D, Oba M, Koyama H, Nishiyama N, Fukushima S, Miyata T, et al. Biocompatible micellar nanovectors achieve efficient gene transfer to vascular lesions without cytotoxicity and thrombus formation. Gene Ther 2007;14(13):1029 38.

[14] Itaka K, Ohba S, Chung U, Kataoka K. Bone regeneration by regulated in vivo gene transfer using biocompatible polyplex nanomicelles. Mol Ther 2007; Epub ahead of print.

[15] Moghimi SM, Symonds P, Murray JC, Hunter AC, Debska G, Szewczyk A. A two-stage poly(ethylenimine)-mediated cytotoxicity: implications for gene transfer/therapy. Mol Ther 2005;11(6):990 5.

[16] Lehmann MJ, Sczakiel G. Spontaneous uptake of biologically active recombinant DNA by mammalian cells via a selected DNA segment. Gene Ther 2005;12(5):446 51.

[17] Varga CM, Tedford NC, Thomas M, Klibanov AM, Griffith LG, Lauffenburger DA. Quantitative comparison of polyethylenimine formulations and adenoviral vectors in terms of intracellular gene delivery processes. Gene Ther 2005;12(13):1023 32.

[18] Hama S, Akita H, Ito R, Mizuguchi H, Hayakawa T, Harashima H. Quantitative comparison of intracellular trafficking and nuclear transcription between adenoviral and lipoplex systems. Mol Ther 2006;13(4):786 94.

[19] Itaka K, Harada A, Yamasaki Y, Nakamura K, Kawaguchi H, Kataoka K. In situ single cell observation by fluorescence resonance energy transfer reveals fast intra-cytoplasmic delivery and easy release of plasmid DNA complexed with linear polyethylenimine. J Gene Med 2004;6(1):76 84.

[20] Goncalves C, Pichon C, Guerin B, Midoux P. Intracellular processing and stability of DNA complexed with histidylated polylysine conjugates. J Gene Med 2002;4(3):271 81.

[21] Lechardeur D, Sohn KJ, Haardt M, Joshi PB, Monck M, Graham RW, et al. Metabolic instability of plasmid DNA in the cytosol: a potential barrier to gene transfer. Gene Ther 1999;6(4): 482 97.

[22] Thellin O, Zorzi W, Lakaye B, De Borman B, Coumans B, Hennen G, et al. Housekeeping genes as internal standards: use and limits. J Biotechnol 1999;75(2-3):291 5.

[23] Jain M, Nijhawan A, Tyagi AK, Khurana JP. Validation of housekeeping genes as internal control for studying gene expression in rice by quantitative real-time PCR. Biochem Biophys Res Commun 2006;345(2):646 51.

[24] Godbey WT, Wu KK, Mikos AG. Poly(ethylenimine)-mediated gene delivery affects endothelial cell function and viability. Biomaterials 2001;22(5):471 80.

[25] Morimoto K, Nishikawa M, Kawakami S, Nakano T, Hattori Y, Fumoto S, et al. Molecular weight-dependent gene transfection activity of unmodified and galactosylated polyethyleneimine on hepatoma cells and mouse liver. Mol Ther 2003;7(2):254 61.

[26] Boeckle S, von Gersdorff K, van der Piepen S, Culmsee C, Wagner E, Ogris M. Purification of polyethylenimine polyplexes highlights the role of free polycations in gene transfer. J Gene Med 2004; 6(10):1102 11.

[27] Regnstrom K, Ragnarsson EG, Koping-Hoggard M, Torstensson E, Nyblom H, Artursson P. PEI-a potent, but not harmless, mucosal immuno-stimulator of mixed T-helper cell response and FasL-mediated cell death in mice. Gene Ther 2003;10(18): 1575 83.

[28] Florea BI, Meaney C, Junginger HE, Borchard G. Transfection efficiency and toxicity of polyethylenimine in differentiated Calu-3 and nondifferentiated COS-1 cell cultures. AAPS PharmSci 2002;4(3):E12.

[29] Hunter AC. Molecular hurdles in polyfectin design and mechanistic background to polycation induced cytotoxicity. Adv Drug Deliv Rev 2006;58(14):1523 31.

[30] Ohba S, Ikeda T, Kugimiya F, Yano F, Lichtler A, Nakamura K, et al. Identification of a potent combination of osteogenic genes for bone regeneration using embryonic stem (ES) cell-based sensor. FASEBj 2007;21(8):1777 87.

Available online at www.sciencedirect.com
ScienceDirect
Reactive & Functional Polymers 67 (2007) 1361–1372
REACTIVE & FUNCTIONAL POLYMERS
www.elsevier.com/locate/react

Study of the quantitative aminolysis reaction of poly(β-benzyl L-aspartate) (PBLA) as a platform polymer for functionality materials

Masataka Nakanishi [a], Joon-Sik Park [b], Woo-Dong Jang [c], Makoto Oba [d], Kazunori Kataoka [a,b,*]

[a] *Department of Materials Engineering, Graduate School of Engineering, The University of Tokyo, 7-3-1 Hongo, Bunkyo, Tokyo 113-8656, Japan*
[b] *Center for Disease Biology and Integrative Medicine, Graduate School of Medicine, The University of Tokyo, 7-3-1 Hongo, Bunkyo, Tokyo 113-0033, Japan*
[c] *Department of Chemistry, College of Science, Yonsei University, 134 Sinchondong, Seodaemun-gu, Seoul 120-749, Republic of Korea*
[d] *Department of Clinical Vascular Regeneration, Graduate School of Medicine, The University of Tokyo, 7-3-1 Hongo, Bunkyo, Tokyo 113-8655, Japan*

Received 30 June 2007; received in revised form 31 July 2007; accepted 2 August 2007
Available online 29 August 2007

Dedicated to Professor Teiji Tsuruta on the occasion of his 88th birthday (Beiju).

Abstract

A facile and quantitative aminolysis of poly(β-benzyl L-aspartate) (PBLA) as well as the solution properties of the prepared cationic polyaspartamide were investigated in this study. The reaction was found to proceed in good yield without undesired side reactions via the formation of a succinimide intermediate in the polymer backbone, which was efficiently converted to polyaspartamide accompanying the α,β isomerization of the main chain. The polarity of solvents and the secondary structure of the polymer strand were closely related to each other in terms of reactivity and stereoselectivity. The aminolysis of PBLA treated with one equivalent amine against benzyl ester groups resulted in the complete conversion at 35 °C in random-coil solvents within 1 h. The racemization that accompanied this reaction was observed in random-coil solvents, but was efficiently suppressed in helicogenic solvents, with 95% of the optical purity maintained in CH_2Cl_2. In addition, the quantitative introduction of *N*,*N*-diisopropylethylenediamine (DIP) led to the formation of cationic polyaspartamide, poly[*N*-(*N*′,*N*′-diisopropylaminoethyl)aspartamide] (PAsp(DIP)), which showed pH and thermo-sensitivities in aqueous media. This systematic investigation of the aminolysis of PBLA with DIP demonstrates the feasibility of a PBLA-aminolysis system for designing functionalized polyaspartamides which can be useful as biomaterials.

Keywords: PBLA; Aminolysis; Quantitative side-chain reaction; Succinimide; Suppression of racemization; pH and thermo-sensitivities

* Corresponding author. Address: Department of Materials Engineering, School of Engineering, The University of Tokyo, Japan. Tel.: +81 3 5841 7138; fax: +81 3 5841 7139.
E-mail address: kataoka@bmw.t.u-tokyo.ac.jp (K. Kataoka).

1381-5148/$ - see front matter © 2007 Elsevier Ltd. All rights reserved.
doi:10.1016/j.reactfunctpolym.2007.08.009

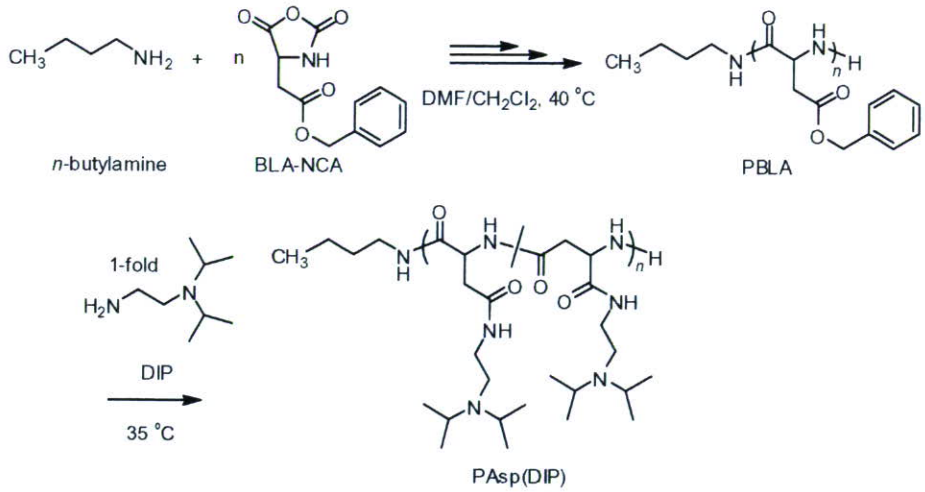

Scheme 1. Synthetic procedures of PBLA and PAsp(DIP) by the successive aminolysis reaction of PBLA.

1. Introduction

Chemical modification by the side-chain reaction of polymer is a convenient way to prepare a variety of functionalized derivatives from a single platform polymer [1–3]. For example, the precursor polymers bearing functional groups such as active ester [4–9], (meth)acryl chloride [10–12], and alkyne [13,14] are typical representatives with a potential for further functionalization or versatile modification according to particular applications. As a rule, the side-chain reaction was considered a facile synthetic route to obtaining polymer analogues with a constant degree of polymerization (DP) and molecular weight distribution (MWD) from a single platform polymer. Thus, the use of precursor polymer as a common intermediate allows for combinatorial strategies, feasible for evaluating and optimizing the correlation between the polymer structure and function.

There have also been many examples in bio-related fields where poly(amino acid)s with high biocompatibility and low toxicity [15–18] were chemically modified to increase their feasibility by binding hydrophobic drugs [19], a hydrophilic ethylene glycol segment [20] and pilot molecules [21] into the side chain. Although there have been several studies on side-chain modification using poly(lysine) or poly(glutamate/aspartate) as a platform polymer, the side-chain reaction of these poly(amino acid)s does not proceed quantitatively. The conversion of all the flanking moieties of the precursor polymers requires extreme conditions such as a high concentration of reactant, high temperature and long reaction time, leading to side reactions such as the decrease of molecular weight (MW) by the cleavage of the amide linkages in the main-chain, as in the case of the aminolysis of Poly(γ-benzyl L-glutamate) (PBLG) [22,23]. Alternatively, poly(succinimide) has been investigated as a more active precursor to preparing the isomeric library of polyaspartamide by the quantitative introduction of the functional groups [24–29]. However, the synthesis of this active precursor has some drawbacks, including a long time reaction, high reaction temperature, and coloring of the obtained product [30,31], limiting the resultant polymer under control. Namely, the polymers are still highly heterogeneous, not only in terms of DP and MWD but also in terms of optical purity and composition of the functional units in the side chain [32,33].

In this regard, we have recently established that the flanking benzyl ester groups of poly(β-benzyl L-aspartate) (PBLA) undergo a quantitative aminolysis reaction with various primary amine compounds, thus offering a variety of polyaspartamides useful for designing polymeric micelles and vesicles as a biomaterial application [34–39]. Although it has been suggested that the mechanism of this unique aminolysis reaction is involved with the succinimidyl ring formation, the details have not yet been clarified. Thus, it is critical to obtain insight into the reaction mechanism, particularly from the standpoint of kinetics, and to identify the detailed structure of polyaspartamide in order to assess its feasibility for use as biomaterials. To this aim, we investigated the mechanism and kinetics of the aminolysis reaction of PBLA, focusing on both the α to β transition

and racemization relevant to the solvent effect and the higher-ordered structure of polymer strands.

In this study, the cationic polyaspartamide was synthesized by reacting PBLA with *N,N*-diisopropylethylenediamine (DIP), and its solubility behavior responsive to pH and temperature was investigated. DIP was selected as a nucleophile to study the aminolysis mechanism and the environmentally responsive properties of polyaspartamide. The primary amino group of DIP was converted to the amide group after the aminolysis of PBLA, and the *N,N*-diisopropylaminoethyl group of DIP was responsible for pH- and thermo-sensitivities (Scheme 1). Among several alkyl groups as a hydrophobic moiety, the isopropyl group was selected with the expectation that a sharp transition of the polymer in aqueous media, like the typical thermoresponsive polymer, poly(*N*-isopropylacrylamide) [40], would occur. In addition, the tertiary amino group with two neighboring isopropyl groups was also selected not only for the hydrophobic-hydrophilic balance between the ionic segment and alkyl segment, but also to exclude undesired cross-linking during the aminolysis. Concerning the kinetics, in general the reactivity of side chains can be controlled not only by the polarity of the solvent but also by the polymer conformation depending on the solvation of side groups, steric hindrances, and the distance of the vicinal groups. From this point of view, we conducted this study in a comparable solvent system for the purpose of evaluating each effect of solvent polarity and polymer conformation on the kinetics and racemization.

2. Experimental

2.1. Materials

β-Benzyl L-aspartate *N*-carboxy-anhydride (BLA-NCA) was obtained from Nippon Oil and Fats (Tokyo, Japan). *N,N*-Dimethylformamide (DMF), 1,4-dioxane (dioxane), dimethylsulfoxide (DMSO), dichloromethane (CH_2Cl_2), and chloroform ($CHCl_3$) were purchased from Wako Pure Chemical Industries (Osaka, Japan) and were purified by distillation according to the conventional procedure [41]. *N,N*-Diisopropylethylenediamine (DIP), *n*-butylamine and triethylamine (TEA) were purchased from Tokyo Kasei Kogyo (Tokyo, Japan) and were distilled from calcium hydride under reduced pressure. The other chemicals were used as received.

2.2. Method

The ^{1}H NMR spectrum was recorded on a JEOL EX 300 spectrometer (JEOL, Tokyo, Japan) at 300 MHz. Chemical shifts were reported in parts per million (ppm) downfield from tetramethylsilane. MW and MWD were estimated using a gel-permeation chromatography (GPC) (TOSOH HLC-8220) system equipped with two TSK gel columns (TSK-gel Super AW4000 and Super AW3000) and an internal refractive index (RI) detector. The columns were eluted with *N*-methyl-pyrrolidone (NMP) containing lithium bromide (50 mM) (0.3 ml min^{-1}) at 40 °C. MW were calibrated with poly(ethylene glycol) standards (Polymer Laboratories, Ltd., UK). The IR spectra were obtained with an IR-550 JASCO spectrophotometer. Gas chromatography (GC) was carried out with GC17A (SHIMADZU, Tokyo, Japan) gas chromatograph equipped with a 30-m long, 250 μm i.d., open tubular column, DB-1 (SHIMADZU GLC, Tokyo, Japan), and a flame ionization detector. C-R7A (SHIMADZU, Tokyo, Japan) was used for instrument control and data acquisition. The carrier gas was hydrogen. The pressure at the head of the column was 400 kPa, and the linear velocity at the end of the column was 41 cm s^{-1}. The sample was injected onto the column at a split ratio of over 25:1. The injection port temperature was 200 °C.

2.3. Synthesis of poly(β-benzyl L-aspartate) (PBLA)

To obtain PBLA (Scheme 1), BLA-NCA (2.49 g, 10 mmol) was polymerized in the mixture of DMF (10.0 mL) and CH_2Cl_2 (100 mL) at 40 °C by the initiation from the terminal primary amino group of *n*-butylamine (14.6 mg, 200 μmol). PBLA was purified by precipitation in ether (3 L) three times, and was confirmed to have a unimodal MWD (M_w/M_n: 1.07) by GPC measurement (Fig. 1C). The DP of PBLA was calculated to be 52 based on ^{1}H NMR spectroscopy (Fig. 1A).

2.4. Synthesis of poly[N-(N',N'-diisopropylaminoethyl)aspartamide] (PAsp(DIP))

Lyophilized PBLA (202 mg, 20 μmol) was dissolved in DMSO (10 mL), followed by the reaction with 1-fold DIP (1 equiv to the residual benzyl ester group in PBLA, 144.3 mg, 1 mmol) under mild anhydrous conditions at 35 °C for 1 h to obtain

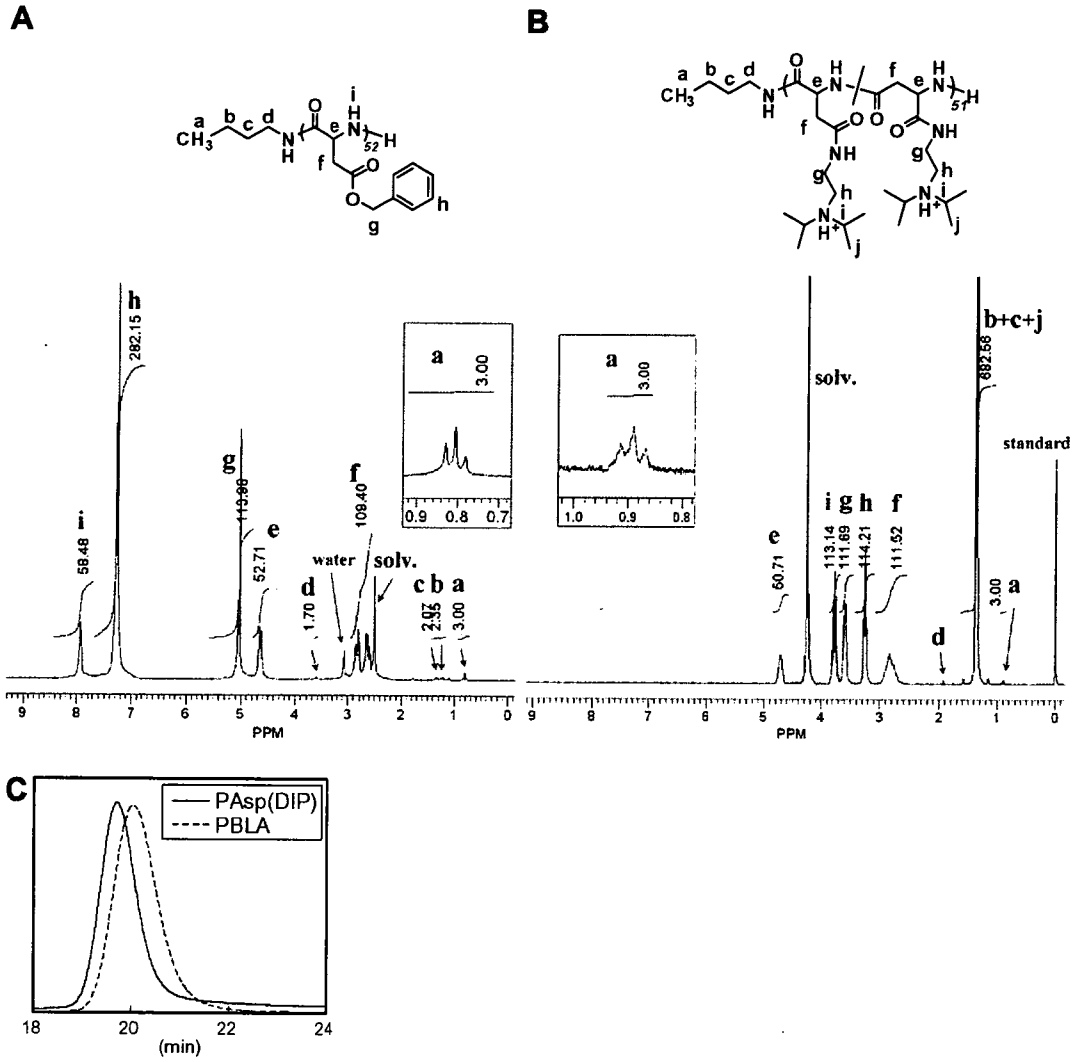

Fig. 1. ^{1}H NMR spectra of (A) PBLA in DMSO-d_6 at 50 °C and (B) PAsp(DIP) synthesized in DMSO in D_2O at 80 °C. (C) GPC diagrams of PBLA and PAsp(DIP) (PEG standard, eluent: NMP (containing 50 mM LiBr), temperature 40 °C, RI detection).

PAsp(DIP). After the reaction, the reaction mixture was slowly added dropwise into a cooled aqueous solution of acetic acid (10% v/v, 40 mL) and dialyzed against an aqueous solution of 0.01 N HCl three times and distilled water one time (molecular weight cut off: 3500 Da). The final solution was lyophilized to obtain the polymer in the chloride salt form with a yield of 92% (221 mg). In addition to the chloride salt form, the unprotonated PAsp(DIP)s were obtained as follows. The reaction mixture was purified by dialysis against DMSO three times and methanol three times. The solution was evaporated *in vacuo* and the polymer was dissolved in benzene, followed by lyophilization. The unprotonated PAsp(DIP) was then obtained as a white powder with a yield of 90% (215 mg). Similarly, the aminolysis of PBLA with DIP was carried out at 35 °C in NMP (reaction time: 1 h), DMF (reaction time: 1 h), $CHCl_3$ (reaction time: 200 h) and CH_2Cl_2 (reaction time: 160 h), respectively. In the case of dioxane, the solution of PBLA in dioxane was at first completely dissolved at 50 °C and then the temperature was allowed to decrease the temperature to 35 °C, followed by the reaction with an equivalent DIP for 260 h. All the yields were approximately 90%. The completion of the aminolysis reaction was confirmed by GC.

2.5. Reaction velocity measurements

The aminolysis of PBLA was carried out using an equivalent DIP at 35 °C in a comparable solvent sys-

tem. The conversion of the BLA residue into the aspartamide residue was calculated from both the remaining amount of DIP and the amount of the benzyl alcohol. The remaining amount of DIP was measured using GC with the internal reference method using *n*-decane as internal standard. PBLA (202 mg) was reacted with 1-fold DIP (144 mg) in 10 mL of solvent. The rate of debenzylation was determined by comparison of the intensity of CH_2 of the leaving benzyl alcohol with that of benzyl ester based on ^{1}H NMR spectroscopy using DMSO-d_6 and CD_2Cl_2 as solvent. PBLA (20.2 mg) was reacted with DIP (14.4 mg) in 1 mL of solvent at 35 °C during the ^{1}H NMR measurement.

2.6. Optical rotation measurements

The specific optical rotation measurements of the polymer samples were carried out in CH_2Cl_2 and DMSO respectively, using a digital polarimeter DIP-370 (JASCO) at a 546 nm wavelength, with a cell of 100 mm length and an integration time of 30 s. The concentration of polymer was adjusted to 1.0 wt% for all the measurements. $[\alpha]_D$ was measured at definite time intervals after adding 1-fold DIP. The measurement was done 20 times for each sample to obtain the average value.

2.7. Analysis of aspartamide enantiomers

The D/L-aspartamide ratios were determined by high performance liquid chromatography carried out by the HiPep Laboratories (Kyoto, Japan) using the enantiomer labeling method (ELAB). This analysis was conducted using a fully automated D/L and quantitative amino acid analyzer, a Shimadzu-CAT Model DLAA-1, which consists of an automated derivatizer with a robot arm, Autoderivat 100/2 of CAT, and a gas chromatograph, Shimadzu Model GC/DLAA with an auto injector, AOC/DLAA, in combination with a chromatographic data processor, Shimadzu Chromatopac C-R4A [42].

2.8. Potentiometric titration and transmittance measurements

PAsp(DIP) (30 mg) prepared in DMF was dissolved in 50 mL 0.01 N HCl and titrated with 0.01 N NaOH added in quantities of 0.063 mL after the pH values were stabilized (minimal interval: 30 s), using an automatic titrator (TS-2000, Hiranuma, Kyoto, Japan) for the titration and transmittance measurements. The pH values and transmittance were measured at 10 °C, 20 °C, 30 °C, 40 °C and 50 °C. The α/pH curves were determined from the titration curves obtained. Each calibration was carried out at the same temperature as each measurement.

3. Results and discussion

3.1. Preparation of PAsp(DIP)

PBLA is known to form the left-handed α-helix in apolar solvents such as dioxane [43], $CHCl_3$ [44], CH_2Cl_2 [45] and the random-coil in polar solvents such as DMF [46] and DMSO [43]. Because of this, these five random-coil and helicogenic solvents with various dielectric constants were selected for this study.

From the ^{1}H NMR measurement, the DP of the PAsp(DIP), comparing the peak intensity ratio of the CH_3 of the *n*-butyl group (**a**) with α-C*H* of PAsp(DIP) (**e**) was calculated to be 51, and it was confirmed that PAsp(DIP) synthesized in DMSO has a unimodal MWD (M_w/M_n: 1.08) by GPC measurement, thus indicating that the aminolysis proceeded quantitatively without causing any cleavage of the main chain (Fig. 1). Similarly, it was confirmed that all the PAsp(DIP)s prepared in other solvents had almost the same MW and a unimodal MWD (Table 1). Therefore, this result demonstrated that the aminolysis of PBLA was a useful side-chain exchanging reaction avoiding the side reaction of the cleavage of the main chain in the appropriate condition.

3.2. Reaction velocity

A significant difference was found in the reaction rate between polar random-coil solvents and apolar helicogenic solvents, as shown in Fig. 2. The reaction was much faster in random-coil solvents than in helicogenic solvents. From a practical point of view, it is worth mentioning that aminolysis with a 1-fold amine is completed after 1 h at 35 °C in polar solvents. In addition, although no difference was found in reactivity among random-coil solvents, the reaction was clearly faster in helicogenic solvents with the increasing dielectric constant of the solvent, suggesting that the rate of the aminolysis reaction of PBLA also depends on the polarity of the solvents. The results of the kinetic studies show that the aminolysis of side-

Table 1
Analytical data of M_w/M_n and L-isomer (%) of PAsp(DIP) synthesized in various solvents

Polymer solvent	PBLA	PAsp(DIP)				
		Dioxane	$CHCl_3$	CH_2Cl_2	DMF	DMSO
ε^a		2.2	4.8	9.1	37	47
$M_w/M_n{}^b$	1.07	1.08	1.07	1.08	1.09	1.08
L (%)[c]	99.9	83.8	89.0	94.5	72.7	73.6

[a] Indicates the dielectric constant of the solvent.
[b] Determined by GPC.
[c] Determined by ELAB method carried out by HiPep laboratories.

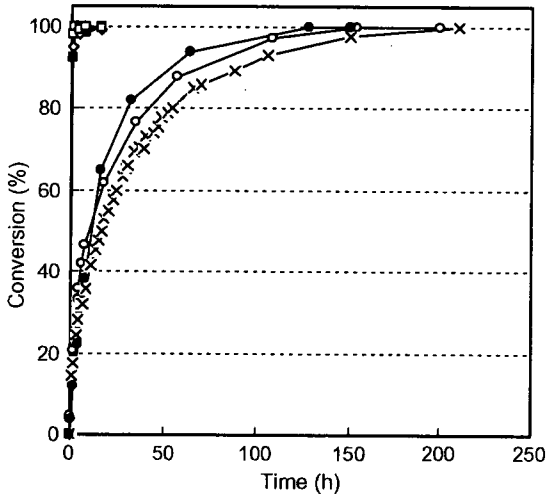

Fig. 2. Time profile of the conversion rate calculated from the remaining DIP in DMSO (□), DMF (◇), CH_2Cl_2 (○) and $CHCl_3$ (×) and the leaving benzyl alcohol in DMSO-d_6 (■) and CD_2Cl_2 (●) in the condition where PBLA reacts with 1-fold DIP at 35 °C.

chain esters of PBLA can be greatly affected by both the conformation of the polymer strand and the polarity of the solvents.

The kinetics data described above suggest that there could be an active intermediate to have this reaction progress rapidly and quantitatively, because the aminolysis of esters, in other words, a way of directly transforming esters to amides, usually requires stoichiometric amounts of promoters or metal mediators [47]. It has been reported that a large amount of primary amines was required to modify all the flanking esters in the side chain of PBLG by aminolysis, and that main-chain scission caused due to the aminolysis of the amide linkage in the main chain by the remaining primary amines [22,23]. In contrast, the stoichiometric aminolysis reaction of PBLA resulted in the prompt and complete conversion in polar and apolar solvents under a mild condition. Of interest is the significant difference in the reaction rate between PBLA and PBLG, because the difference between their primary structures is the presence or absence of γ-CH_2 in the side chain. Blout et al. [46] reported the formation of poly(succinimide), an active precursor polymer, from PBLA when PBLA was treated with catalytic amounts of base in DMF or DMSO. The formation of poly(succinimide) was determined by isolation and comparison with the infrared spectra reported in the literature [46]. However, the treatment of PBLG under identical conditions showed no evidence of cyclization to poly(glutarimide) [46]. Therefore, the mechanism by which α to β isomerization of aspartic acid occurs was focused here in order to understand the mechanism by which the aminolysis of PBLA occurs. Moreover, there have been many reports showing that the racemization of aspartic acid and asparagine residues was accelerated via succinimide intermediates [48–53]. From this result, it is highly expected that the racemization occurs when the succinimide formation occurs.

For the reasons mentioned above, it is estimated that there are three stages: (1) ring formation, (2) racemization, (3) aminolysis in the present reaction of PBLA (Scheme 2). The reaction rate constants of each stage were defined as k_1, k_2 and k_3, respectively. In the first stage, the aminolysis of PBLA starts with the activation of the nitrogen atom in the main chain by an amine as a weak base coordinating the proton of the amide group, and then the nucleophilic attack by the activated nitrogen on the carbon atom of the carbonyl group in the side chain occurs to form the succinimidyl ring. The eliminated proton which recombines with the benzyloxyl group is released as benzyl alcohol, accompanying the regeneration of amine. Therefore, the ring formation is expected to be a catalytic reaction. In the second stage, the proton in the α-position is easily eliminated with ease in the succinimidyl ring, and then racemization proceeds by the keto–enol tau-

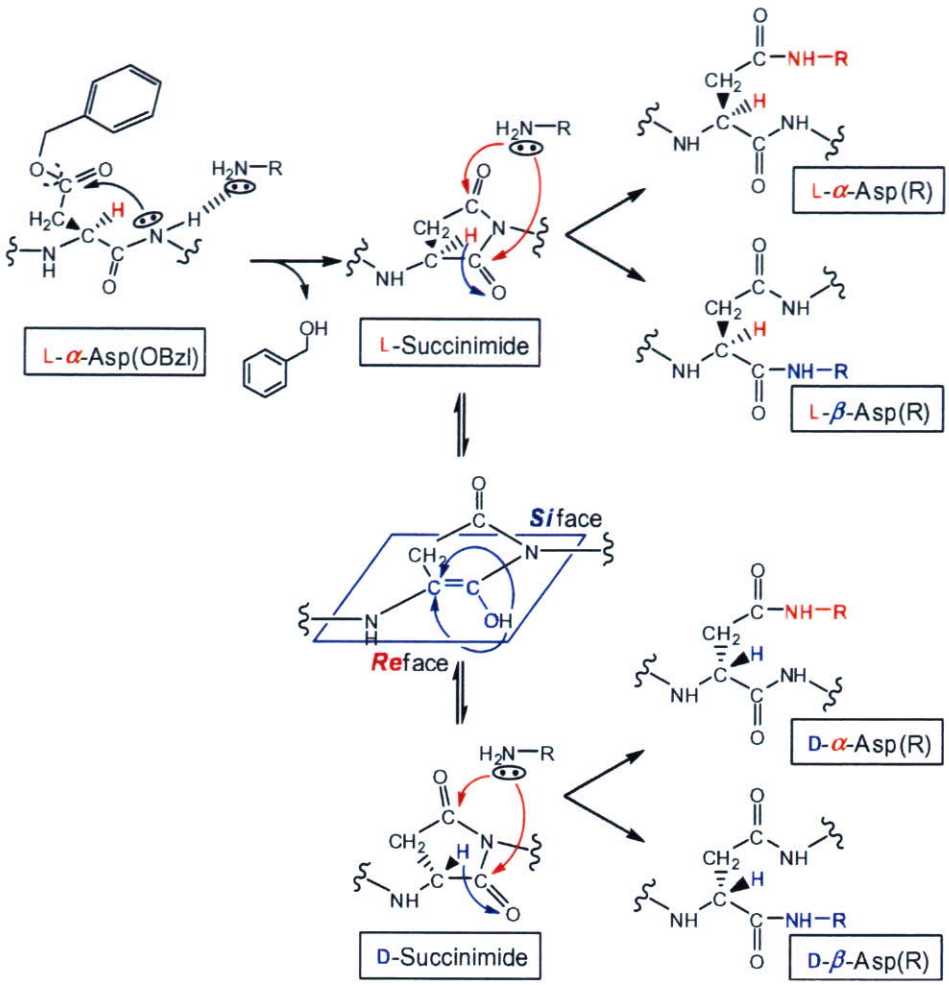

Scheme 2. Mechanism of aminolysis reaction of PBLA.

tomerism. In the third stage, an amine undergoes a nucleophilic attack to one of two carbonyl groups in the succinimidyl ring, which is efficiently converted to the isomerization to form the α,β-aspartamide.

Therefore, the aminolysis of PBLA by less than a 1-fold amount of DIP in DMSO($-d_6$) or CH_2Cl_2 (CD_2Cl_2) was performed to confirm whether aminolysis proceeds via the formation of the succinimide

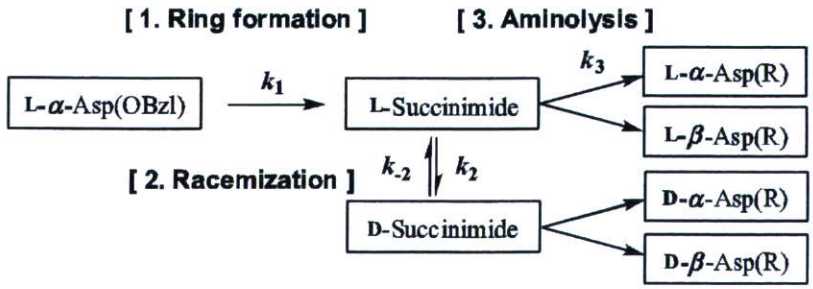

intermediate or not. In addition, the degree of racemization after the aminolysis of PBLA with 1-fold DIP was analyzed.

3.3. Identification of intermediate structure and kinetics

3.3.1. Identification of intermediate structure and kinetics in DMSO

The confirmation of an intermediate structure was done in the condition where PBLA reacted with 0.5-fold DIP in DMSO-d_6 using ^{1}H NMR spectroscopy recorded after 0.5 h, 1 h and 6 h (Fig. 3). It was determined that a 0.5-fold amount of DIP was added to this system by comparing the intensity of CH_3 (**j**) of DIP with that of CH_2 (**c**) of the benzyl group of PBLA. The sharp peak of CH_2 (**f**) of the leaving benzyl alcohol appeared at 4.5 ppm, and the intensity increased promptly in association with the separation of the peak (**d**) due to the benzyl alcohol. The integration value of CH_2 (**f**) of the benzyl alcohol became ca. 2 at 1 h. This is consistent with the complete disappearance of the peak corresponding to CH_2 (**c**) of the benzyl group of PBLA within 1 h. Thus, it was confirmed that the debenzylation was completed within 1 h. It was also confirmed by GC that all the DIP were consumed after 6 h.

Comparing the spectrum of PBLA (A) with that of the reactant at 0.5 h (B) in Fig. 3, it is worth noting the substantial shift of the α-C*H* (**a**) peak at 4.7 ppm. Concomitantly, the peak assigned to β-CH_2 seems to shift from 2.6 and 2.8 ppm (**b**) to 2.7 and 3.2 ppm (**l**), respectively, suggesting the substantial change in the main chain structure. Furthermore, the appearance of new peaks at 5.3 (**k**) and 5.1 (**m**) ppm was clearly observed. For further analysis, each intensity and the summation of the two peaks (**k**) and (**m**) from (B) to (D) in Fig. 3 were compared. According to the reported chemical shift values of poly(succinimide) [54], the peaks (**k**) and (**l**) were assigned to α-C*H* and β-CH_2, respectively, of the succinimide ring produced in the main chain. In accordance with the gradual decrease in the peak intensity of peak (**k**) with time, an alternative increase in the intensity for peak (**m**) was observed, suggesting the progress of the aminolysis reaction. Note that the summation of the peak intensities of (**k**) and (**m**) always took the constant value of 1.1 after 1 h. Therefore, it is reasonable to conclude that the peak (**m**) is assigned to α-C*H* of polyaspartamide. The time-trace of the ^{1}H NMR spectra revealed that the aminolysis reaction successively occurred after the prompt progress of succinimide formation ($k_1 > k_3$) in DMSO.

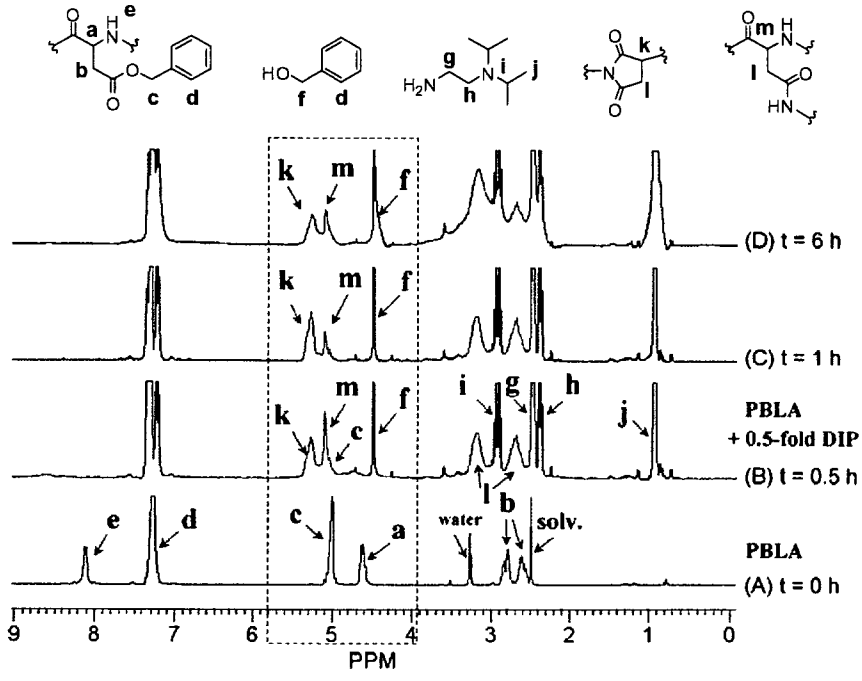

Fig. 3. Time-trace of ^{1}H NMR spectra of PBLA reacting with 0.5-fold DIP in DMSO-d_6 at 35 °C.